

The 2012–2013 Montes Claros earthquake series in the São Francisco Craton, Brazil: new evidence for non-uniform intraplate stresses in mid-plate South America

Hans Agurto-Detzel,¹ Marcelo Assumpção,¹ Caio Ciardelli,¹
Diogo Farrapo Albuquerque,² Lucas V. Barros² and George S. L. França²

¹Institute of Astronomy, Geophysics and Atmospheric Sciences, University of São Paulo, São Paulo, 05508-090, Brazil. E-mail: h.agurto.detzel@gmail.com

²Seismological Observatory, University of Brasilia, Brasilia, 70910-900, Brazil

Accepted 2014 August 29. Received 2014 August 28; in original form 2014 March 11

SUMMARY

On 2012 May 19, an $m_b = 4$ earthquake shook the town of Montes Claros, Brazil in the middle of the São Francisco Craton. Because of the scarce seismicity in the area, an event like this could provide valuable information to characterize the governing seismotectonics and stress field for the region. Here, we present the results of more than 1 yr of local seismic monitoring after the main shock. We found that the seismicity originated at approximately 1-km depth in an NNW-oriented blind reverse fault, dipping to the E. The magnitude of the main shock was $4m_b$, with aftershocks reaching up to $3.6m_b$. Focal mechanisms from first motion polarities and waveform moment tensor inversions indicate a reverse faulting in agreement with the orientation of the aftershock locations. In addition, we derived a new 1-D local velocity model using a simultaneous inversion of hypocentres and velocity layers. The results indicate P -wave velocities of 4.5 km s^{-1} for the upper layer of carbonate rocks and 5.23 and 5.69 km s^{-1} for the lower fractured and compact crystalline basement layers, respectively. Higher V_p/V_s ratios were obtained for the upper two layers compared to the lowermost layer, possibly indicating presence of rock fracturing and percolated water. The calculated stress drop for the main event is 0.33 MPa , which is a relatively low value for an intraplate earthquake but still within the observed range. The inversion of the main shock focal mechanism and previously published focal mechanisms suggests a compressional stress regime in the central part of the São Francisco Craton, which is different from the strike-slip regime in the southern part, although both have an EW-oriented σ_1 . On the other hand, focal mechanisms of events located to the west of the craton indicate an NW–SE oriented σ_1 for central Brazil. This variability highlights the importance of local sources of stresses (e.g. flexural stresses) in mid-plate South America, unlike other mid-plate areas of the world, such as central and east North America, where a more uniform stress field is observed.

Key words: Seismicity and tectonics; Intraplate processes; Cratons; Dynamics; Seismotectonics; Neotectonics; South America.

1 INTRODUCTION

Given that one of the most direct pieces of evidence of stress release in the crust is the occurrence of tectonic earthquakes, focal mechanisms constitute a common data source for stress field characterization. Borehole breakouts are also often used to measure the orientation and relative magnitudes of the principal stress axes, but in absence of these types of measurements, a set of reliable focal mechanism solutions is necessary. A major difficulty to character-

ize intraplate stresses in mid-plate South America is the limited quantity of known focal mechanisms caused by the scarce seismicity ($M > 4$) in this area. In addition, the sparse station coverage prevents the use of events with smaller magnitudes. Only a handful of studies on the regional stress field exist (e.g. Assumpção *et al.* 1985; Assumpção & Suárez 1988; Assumpção 1998a,b), and few focal mechanisms and other types of measures, such as borehole breakouts and other *in situ* measurements, have been published for this region. Thus, it is important to maximize the use of any new

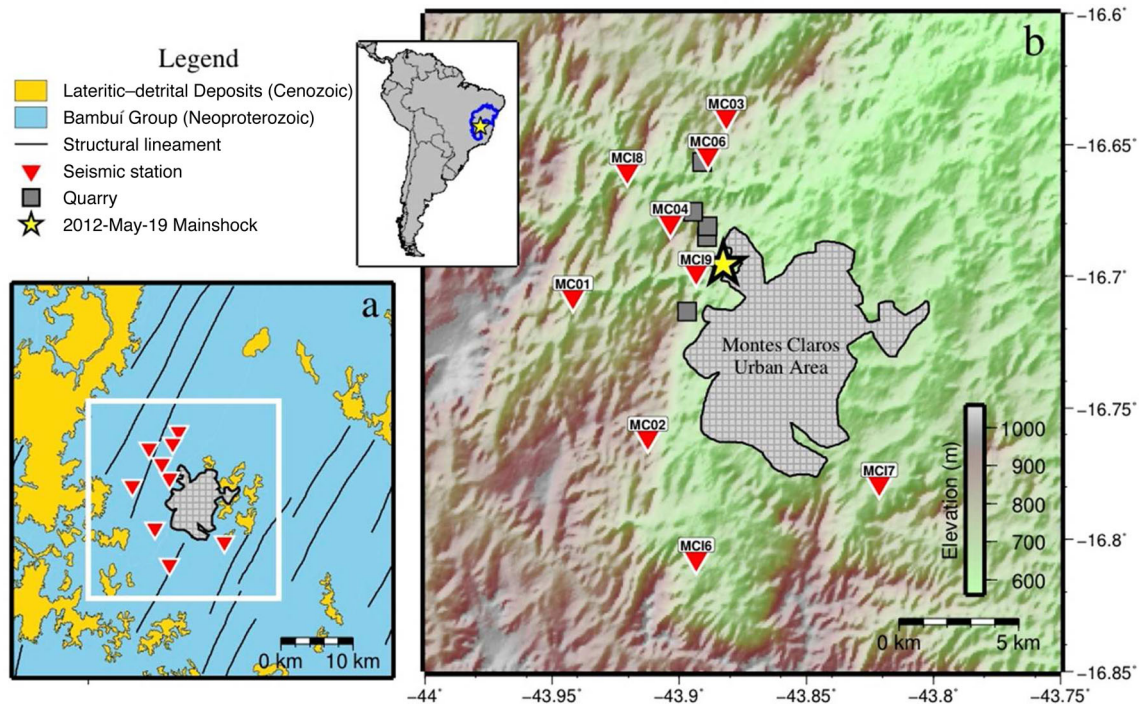


Figure 1. Location of the study area. (a) Simplified geology; modified from Heineck *et al.* (2004). White square indicates area on figure (b). (b) Location of the study area and seismic network. Inset: Location of the main shock in South America. The blue line delimits the São Francisco Craton.

seismological data for this area of Brazil that could lead to a better understanding of the dominant seismotectonics and stress field in mid-plate South America.

On 2012 May 19, an $M = 4$ earthquake struck the town of Montes Claros, Minas Gerais, Brazil, in the middle of the São Francisco Craton. Shortly after this main event, a temporal local seismic network composed of nine broad-band seismometers was installed in the nearby area by the Universities of Brasília and São Paulo to study the aftershock activity. In this paper, we show the results of that survey, which involved determining the magnitudes for the largest events, calculating a 1-D local velocity model for the area, accurately relocating the aftershocks using waveform correlation, computing focal mechanisms from first motion polarities and moment tensor waveform inversions, calculating stress drops and inverting the regional stress field using the 2012 Montes Claros main shock and previously published focal mechanisms for central-east Brazil. We want to answer the following questions: what was the origin and nature of the 2012–2013 Montes Claros seismic sequence and what can this seismicity tell us about the dominant stress field in central-east Brazil compared to other mid-plate areas of the world.

Previous studies found reverse faulting seismicity in the area immediately north of the Montes Claros sequence (e.g. Assumpção *et al.* 1990; Lopes 2008; Chimpliganond *et al.* 2010) in the São Francisco Craton (Fig. 1). This seismicity was associated with the expected average E–W compressive stress regime in Brazil, tentatively proposed by Assumpção (1992, 1998b). In addition, in a compressional stress regime, intraplate earthquakes tend to occur because of the reactivation of pre-existing zones of weakness (e.g. Talwani & Rajendran 1991). We hypothesize that the seismicity of the 2012 sequence corresponds to reverse fault events directly linked to the current E–W compressive regime in the central part of the São Francisco Craton, similar to the northern seismicity. We will show that this earthquake is part of the expected accommodation of stresses in the area and can be explained as the tectonic

response to the stress field produced by plate-scale tectonic forces, similar to other published seismic events in the craton. Nonetheless, the focal mechanisms west and south of the craton suggest a more heterogeneous stress field for mid-plate South America, indicating a significant contribution of local sources of stress.

1.1 Geotectonic setting

The stable South American platform mainly formed by the agglutination of Precambrian cratonic masses during the Brasiliano orogeny from *ca.* 750 to *ca.* 540 Ma (Almeida *et al.* 2000). Our study area is situated in the São Francisco Craton, central-east Brazil, which is one of the biggest Precambrian cratons, only exceeded in size by the Amazonian Craton (Cordani *et al.* 2000; Fig. 1 inset). The geology of the area consists of very low to low-grade Neoproterozoic metamorphic rocks belonging to the Bambuí Group, deposited over the crystalline cratonic basement. This basement is comprised mainly of Arquean terranes of granitic/gneissic rocks. The Bambuí Group is represented by the Serra de Santa Helena, Lagoa do Jacaré and Serra da Saudade formations, which mainly consist of limestones, siltstones and argillites (Heineck *et al.* 2004; Chaves *et al.* 2011). The occurrence of carbonate rocks is highlighted in the area by the presence of several quarries near the urban area of Montes Claros (Fig. 1). Structurally, the zone is dominated by NE lineaments, including thrust and reverse faults.

1.2 The 2012 Montes Claros earthquake and its context in the Brazilian seismicity

Located in the stable continental interior of the South American Plate, Brazil is characterized by low levels of seismicity

Table 1. Largest events of the Montes Claros sequence.

| Event no. | Date | Time (UTC) | Latitude | Longitude | Depth | m_R |
|-----------|------------------|-------------|----------|-----------|-------|-------|
| 1 | 2011 March 5 | 23:28:44.10 | -16.6950 | -43.8834 | – | 3.3 |
| 2 | 2012 May 19 | 13:41:22.56 | -16.6955 | -43.8848 | 1.1 | 4.0 |
| 3 | 2012 December 19 | 04:54:38.50 | -16.6967 | -43.8808 | 1.4 | 3.6 |
| 4 | 2012 December 19 | 05:31:16.83 | -16.6984 | -43.8799 | 1.4 | 3.6 |
| 5 | 2013 April 18 | 10:10:52.00 | -16.6968 | -43.8885 | 1.5 | 3.5 |
| 6 | 2014 April 6 | 13:39:29.60 | -16.6877 | -43.8902 | 1.9 | 3.3 |
| 7 | 2014 April 6 | 19:31:05.30 | -16.6853 | -43.8883 | 2.0 | 3.3 |

(magnitude 5 occur only once every 4 yr) and shallow crustal depths (mostly <10 km; Berrocal *et al.* 1984; Assumpção *et al.* 2014). The largest recorded event in this stable region was the 1955 $m_b = 6.2$ Serra do Tombador earthquake (Barros *et al.* 2009), which is at least one magnitude unit less than the largest recorded magnitude in other stable continental interiors in the world (e.g. India, North America; Johnston 1989). South of 15°S, seismicity in Brazil tends to concentrate offshore in the continental shelf rather than onshore in the continental interior (Assumpção 1998b; Assumpção *et al.* 2014). At this latitude, inland Brazil is not exempt from important seismic activity, such as the 2007 $m_b = 4.9$ Caraíbas-Itacarambi earthquake, which caused the first death from an earthquake in Brazil (Chimpliganond *et al.* 2010).

Seismicity near Montes Claros is not a new occurrence. The Brazilian Seismic Bulletin (<http://www.moho.iag.usp.br/portal/events>) reports seismic activity up to $m = 3.7$ in this region as early as 1978 (see Supporting Information Table S1). Recent major activity ($m > 3$) has been detected since 2011 March when an $m_R = 3.3$ event was recorded. This event was recently relocated by C. Ciardelli (personal communication, 2014) using cross-correlation of Lg waves, which resulted in an epicentre within approximately 200 m of the 2012 May main shock. More recently, seismic activity was reactivated in 2014 April with two important earthquakes $m_R = 3.3$ (Table 1).

The earthquake on 2012 May 19 shook the town of Montes Claros at 10:40 local time, causing alarm among the local population and minor damage to several poorly built houses (intensity V–VI MM; Albuquerque *et al.* 2012; Assumpção *et al.* 2013). This earthquake, $m_R = 4$, was the largest of the sequence, with major aftershocks ($m > 2.9$) in 2012 September and December, 2013 April and 2014 April. No active fault has been recognized in the epicentral area, which is surrounded by limestone quarries that often produce controlled explosions. No relationship has been established

regarding these detonations as a mechanism to induce the observed seismicity.

2 DATA AND METHODS

A temporary local seismic network was deployed 1 week after the 2012 May 19 main shock (Figs 1 and 2). Four stations were installed by the University of São Paulo and five by the University of Brasília. All of the stations had broad-band seismometers continuously recording at a sampling rate of 100 or 200 sps. The network operated from 2012 May to 2013 June, but for the last 5 months, only three stations (MCI6, MCI8 and MCI9) remained active (Fig. 2). Additional data from the Brazilian Seismic Network (Pirchiner *et al.* 2011) were used to analyse the main shock and larger aftershocks.

The continuous recording was visually examined in search of aftershocks. A total of 304 events were detected and located using the Hypocentre code (Lienert & Havskov 1995) from the software package SEISAN (Havskov & Ottemöller 1999). *P*- and *S*-phases were manually picked totalling 1288 *P*- and 1228 *S*-arrivals. Magnitudes for the larger events were calculated using the regional magnitude scale m_R based on maximum *P*-wave particle velocity (Assumpção 1983). M_W and focal mechanisms were obtained using waveform moment tensor inversion (see below).

The hypocentre of the 2012 May 19 main shock was located using regional stations belonging to the Brazilian Seismic Network and then relocated using relative locations and data from the local network. One of the large aftershocks ($m_R = 2.9$) recorded by the local network and regional stations was used as the reference event. *P*- and *S*-wave arrivals were determined using waveform cross-correlation. The station residuals of the reference event at the regional stations were then used as station corrections to relocate the main event more accurately (Assumpção *et al.* 2013).

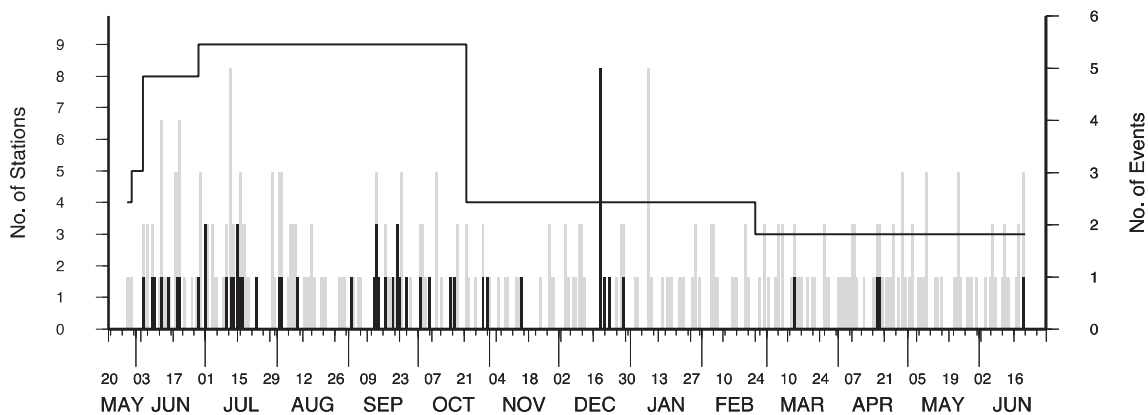


Figure 2. Histogram showing the temporal evolution of the sequence. The grey bars depict the total daily number of events (including quarry blasts); black bars indicate tectonic events (right axis). The solid black line indicates the number of active seismic stations (left axis).

3 RESULTS

3.1 Velocity model inversion

The preliminary locations of the initial 304 detected events were used to extract a high-quality subset according to number of observations (>6) and station azimuthal gap ($<180^\circ$). This subset, which was composed of 102 high-quality events (531 *P*- and 503 *S*-phases), was then introduced into a simultaneous inversion (software VELEST; Kissling *et al.* 1994) of hypocentres and velocity model. Initial velocity models were randomly created to derive a new 1-D velocity model for the area, including station corrections. The initial velocity model was taken from Chimpliganond *et al.* (2010) concerning a seismic sequence in Caraíbas-Itacarambi (approximately 180 km north of our study area) because of the proximity and similarity of the geology in both areas. Depths and thicknesses of the layers were fixed, and only velocities were simultaneously inverted with the hypocentral locations.

The results of the 1-D velocity model inversion show *P*-wave velocities of 4.5 km s^{-1} for the upper layer of carbonate rocks (Bambuú group), while the lower layers composed by fractured crystalline rocks and compact gneiss present *P*-wave velocities of 5.23 and 5.69 km s^{-1} , respectively (Fig. 3 and Table 2). The V_p/V_s ratio for the upper two layers indicates values of 1.72 and 1.75, respectively. The compact gneiss layer has a $V_p/V_s = 1.65$. The higher V_p/V_s ratios of the upper two layers most likely indicate the degree of fracturing in the rocks and possible percolated water. The average V_p/V_s ratio calculated for the area from a composite Wadatti diagram is 1.67 (see Fig. S2). The rms traveltimes residual of the inversion performed with the new velocity model decreased from an initial 0.046 to 0.035 s after the simultaneous inversion.

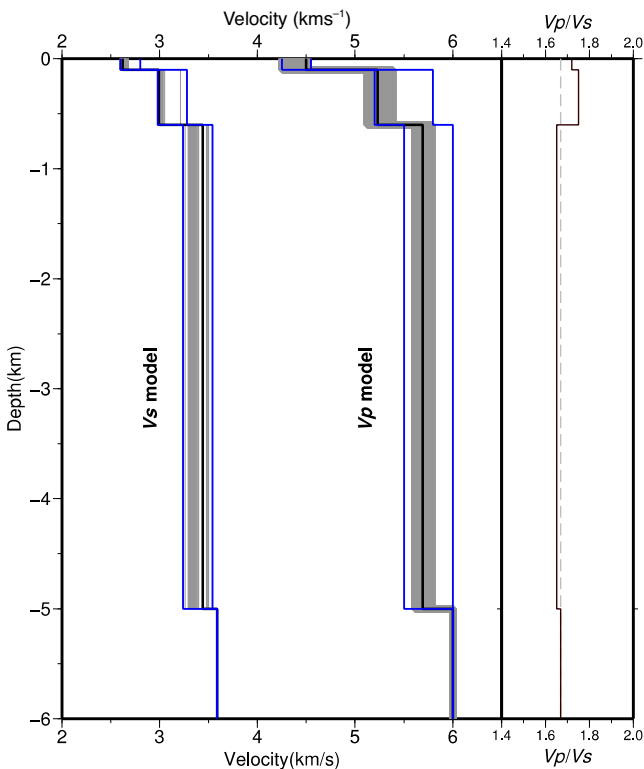


Figure 3. *P*- and *S*-wave velocity models obtained from the simultaneous inversion. Blue lines show the range of the initial models, grey lines are the best 5 per cent of final models and the thick black line indicates the best final model. V_p/V_s ratio results are shown to the right.

Table 2. Final 1-D velocity model. Depth is indicated as the top of each layer. * denotes values that were kept fixed during the inversion.

| Depth (km) | V_p (km s $^{-1}$) | V_s (km s $^{-1}$) | V_p/V_s | Lithology |
|------------|-----------------------|-----------------------|-----------|--------------------|
| 0.0 | 4.50 | 2.62 | 1.72 | Bambuú Group |
| 0.1 | 5.23 | 2.99 | 1.75 | Fractured Basement |
| 0.6 | 5.69 | 3.44 | 1.65 | Compact Basement |
| 5.0 | 6.00* | 3.59* | 1.67* | Half-Space |

3.2 Aftershock relocations and waveform correlation

The 2012 May 19 main shock was located to the northwest of the Montes Claros urban area at a depth of 1.1 km. According to the available literature, no active fault has been previously recognized in this area. The magnitude estimated by the National Earthquake Information Center (NEIC) catalogue was $m_b = 4.1$, while the regional magnitude was $m_R = 3.9$. Because m_b and m_R present equivalent magnitudes (Assumpção 1983; Assumpção *et al.* 2014), we averaged the final magnitude for this event to be $m = 4.0$.

The hypocentral aftershock locations using our new velocity model show two clearly differentiated groups of events: (1) related to quarry blasts and (2) natural seismicity (Figs 4 and S3). Approximately 85 per cent of the processed events consisted of controlled explosions associated with mining activities in the area. These events are easily discernible because of their spatial association with quarries, occurrence during working hours and high-frequency/low-amplitude waveforms (Figs S3 and S7). Another group of small events (occurred from 2012 June 6 to August 15 with magnitudes <1) was located to the south of the Sobritas quarry. Although these events are not spatially related to any known quarry, they occurred on weekdays during working hours and are most likely associated to man-made activities.

The natural seismicity occurs mostly in the first 7 months after the main shock, with peaks of activity in 2012 September and December associated with three of the larger aftershocks (Fig. 2). Another large earthquake was recorded in 2013 April with a magnitude of $m_R = 3.5$ (see Table 1).

To accurately relocate the subset of natural seismicity (39 events located with a minimum of four stations), we correlated both *P*- and *S*-phases to obtain new corrected arrival times. In this way, we attempted to minimize picking errors and relative location uncertainties, particularly for small events with low signal-to-noise ratios. Our waveform correlation algorithm calculates time corrections for the manually picked *P*- and *S*-phases by correlating their waveforms within a pre-defined time window around the phases. A ‘branched’ correlation method (Ciardelli *et al.* 2014) was implemented, in which a previously defined reference event, in our case the largest of the series, is correlated with the ‘most similar’ event of the sequence in terms of correlation coefficient. This correlated event is then transferred to a group of reference events. The correlation process then continues looking for a third event that is most similar to one in the reference group. The process iterates until all of the events have been correlated and transferred to the reference events group. The result is a new set of corrected *P*- and *S*-phases, which is then used to accurately relocate the seismicity, allowing for better imaging of the fault plane geometry.

Fig. 4 shows the relocated seismicity after the waveform correlation, indicating a rupture area (given by the aftershocks distribution) of approximately $1.5 \times 1.5 \text{ km}^2$, with hypocentres occurring between 0.5 and 1.5-km depth. The hypocentral locations define a plane striking 347° , and dipping 30°NE , which agrees with the fault planes obtained from first motion polarities and moment tensor

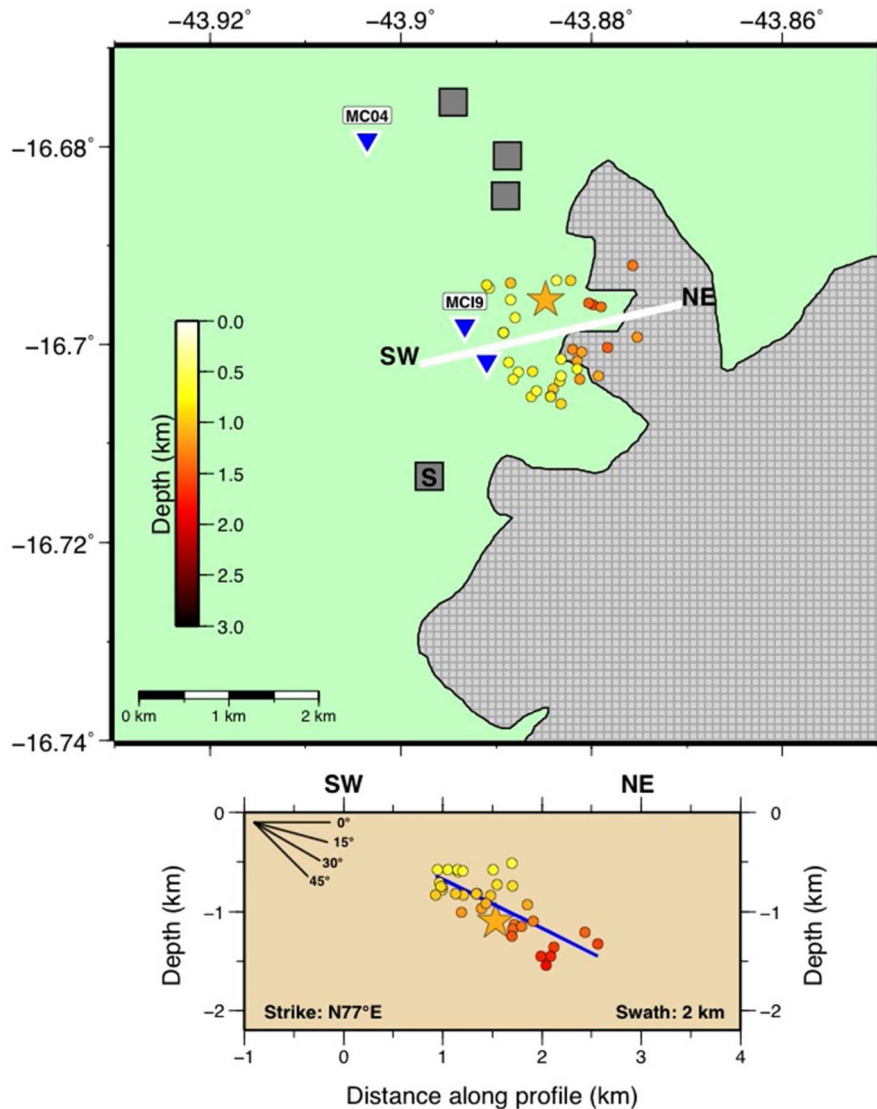


Figure 4. Relocated natural seismicity after waveform correlation. S = Sobritas quarry. The white line indicates the depth profile SW–NE. The blue line shows the best-fitted fault plane. Other features are the same as Fig. 1.

inversions. Noteworthy is the patch-like distribution of the events on the plan view map showing a lack of aftershocks in the area immediately south of the main shock epicentre. In this case, the main shock rupture would have initiated in the northern part of the patch and extended to the south along the fault plane. In any case, these assumptions must be carefully observed given the location uncertainties (approximately 300 m for the relocated aftershocks) and low magnitude of the main event.

3.3 Focal mechanisms and waveform moment tensor inversions

Unfortunately, it was impossible to perform waveform moment tensor inversion for the main shock given that the nearest available station was 300 km away, and the data poorly fit the synthetic seismograms because of the low signal/noise ratio. Instead, a composite focal mechanism for this event was computed from *P*-wave first motion polarities using observations registered at regional and temporary local stations from the main shock and three of the larger af-

tershocks, assuming they had the same faulting mechanism (Fig. 5). This assumption is justified by the consistency of the polarities and similar results obtained using waveform moment tensor inversions of the aftershocks (see below).

A total of 24 first motion polarity observations were used to constrain the composite focal mechanism for the main shock. Of the 24 observations, five correspond to regional stations and 19 to local stations. The best solution indicates reverse faulting with nodal planes (strike/dip/rake) 347/50/135 and 110/57/50, and a nearly horizontal *P* axis trending NE–SW (Figs 5 and 6). The distribution of the aftershocks agrees with the first of these planes (Fig. 4), implying that this is the fault plane. Thus, the main shock rupture corresponds to a reverse fault striking NNW and dipping east.

Full waveform moment tensor inversions were performed for some of the larger aftershocks to obtain their focal mechanisms and moment magnitudes. The software ISOLA (Sokos & Zahradnik 2008) was used for this instance because of its simplicity and usefulness to process local events. After removing the instrument response, the waveforms were bandpass filtered between 0.4 and 1.2 Hz. For each event, we used a fixed epicentral location and

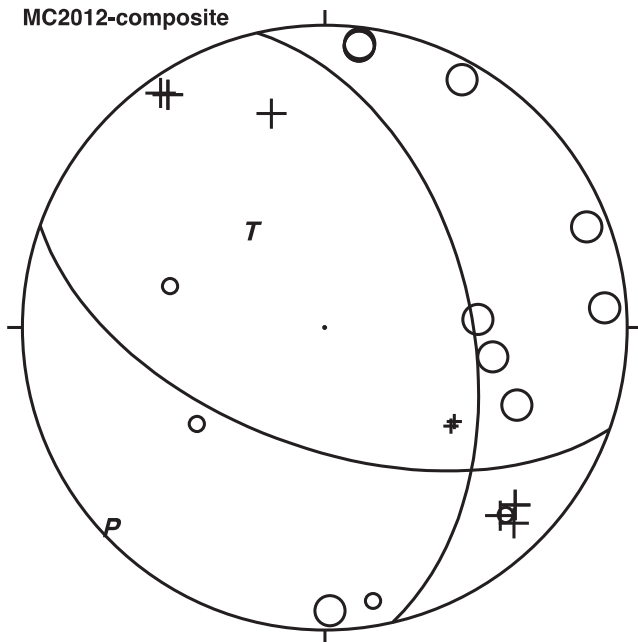


Figure 5. Composite focal mechanism calculated for the 2012 May 19 main shock. Open circles and crosses are dilatational and compressional polarities, respectively. The size of symbols are proportional to the quality of the polarity reading. *P* and *T*-axes are shown.

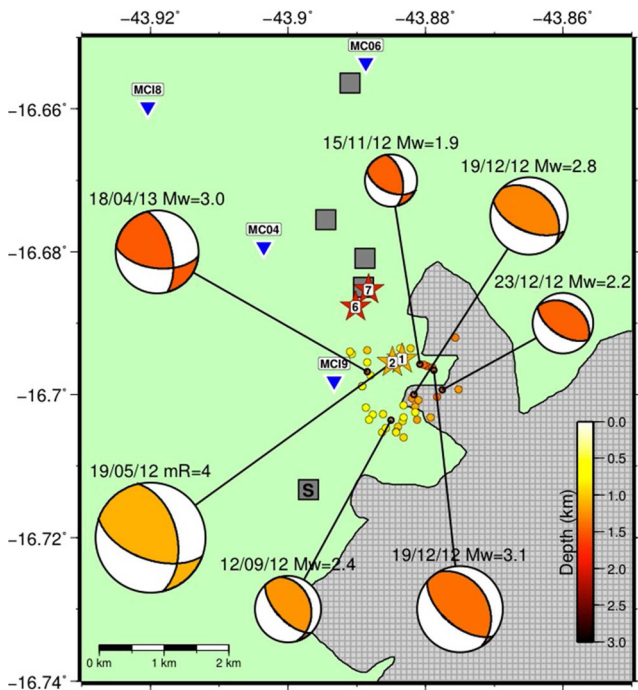


Figure 6. Natural seismicity and focal mechanisms. Stars with numbers indicate the larger events according to Table 1. Other features are the same as Fig. 4.

grid-searched the best depth and centroid time based on the correlation between their real and synthetic waveforms. All of the events were inverted for a deviatoric moment tensor inversion, that is, each solution is composed of a double couple (DC) and a compensated linear vector dipole (CLVD) part.

Some problems were faced to obtain reliable moment tensor solutions for some of the aftershocks, including the unavailability

Table 3. Orientations (strike/dip/rake) and magnitudes of calculated focal mechanisms. * denotes calculated from low-frequency spectral level at regional stations (Stéphane Drouet, personal communication, 2013).

| Event | Fault plane | Aux. plane | M_W | m_R |
|-------------------------|-------------|------------|-------|-------|
| 2012 May 19 13:41 | 347/50/135 | 110/57/50 | 3.3* | 4.0 |
| 2012 September 12 23:56 | 345/31/115 | 137/62/76 | 2.4 | 2.9 |
| 2012 November 15 03:03 | 348/54/130 | 112/52/48 | 1.9 | 2.3 |
| 2012 December 19 04:54 | 330/34/107 | 130/58/79 | 3.1 | 3.6 |
| 2012 December 19 05:31 | 316/35/109 | 113/57/77 | 2.8 | 3.6 |
| 2012 December 23 06:06 | 304/33/091 | 123/57/90 | 2.2 | 2.7 |
| 2013 April 18 10:10 | 346/62/142 | 097/57/35 | 3.0 | 3.5 |

of all of the stations and near-field effects on the seismograms such as tilting for the bigger aftershocks and noisy signals for the smallest events. However, we successfully obtained moment tensors for six of the larger aftershocks, all with reverse faulting mechanisms, similar to the orientations obtained for the main shock (Fig. 6). The moment magnitudes range from 1.9 to 3.1 M_W , which suggests a relationship of $M_W \approx m_R - 0.5$ for this sequence of events (see Table 3). Figs S4–S6 show examples of the waveform fitting for some of these inversions.

4 DISCUSSION

Inferred from the spatial occurrence and faulting mechanisms of the seismic events, the 2012–2013 Montes Claros seismic sequence had a tectonic origin related to a seismogenic NNW-striking reverse fault dipping east. Other events detected by the local network correspond to controlled quarry blasts, which would not be related to the origin or permanence of the natural seismicity in the area. These explosions are caused by mining activities in carbonate rock quarries to the west of the town and their locations help constrain an independent estimation of the location error, which for the case of the Sobritas quarry is approximately 200 m. However, we could not use these explosions to better constrain the local velocity model because there is no independent information regarding the timing of the blasts.

It is also interesting to analyse the temporal evolution of the sequence. The controlled blasts occurred during the observation period without any distinctive pattern, but the natural seismicity occurred mostly during the first 7 months of aftershock activity (Figs 2 and S3a). By plotting the events according to hour of occurrence (Fig. S3b), we can easily discern between artificial events that occur in the afternoon/evening hours, and natural seismicity that occurs during any time of the day.

The natural seismicity is mostly located between 0.5 and 1.5 km depth, therefore nucleating in the crystalline basement (gneiss). No structure like the one imaged by this seismicity had been previously recognized in this area. In addition, because of the depth and low magnitude of the events, a rupture would likely not reach the surface. This was confirmed by field observations on the projected site where the fault plane would have ruptured the shallow layers (Manoel Leite, personal communication, 2013). The length of the rupture area given by the disposition of the aftershocks would be approximately 1.5 km, which is larger than estimations from scaling relationships by Wells & Coppersmith (1994) for an $m = 4$ earthquake (only 0.8 km), but matches the width of 1.6 km predicted by the relationship proposed by Nuttli (1983) for intraplate earthquakes.

It has been proposed that intraplate earthquakes have stress drops approximately two to three times greater, on average, than interplate

earthquakes (e.g. Kanamori & Anderson 1975; Allmann & Shearer 2009; Viegas *et al.* 2010). Considering the extension of the aftershocks during the first 7 months of the sequence, we determined a circular rupture area of approximately 1.4 km². Using the equation $\Delta\sigma = C^*M_0/A^{1.5}$ (Aki 1972), where C^* is a constant of value 2.4 for a circular crack (Eshelby 1957), M_0 is the seismic moment and A is the fault area, we can calculate the stress drop ($\Delta\sigma$) of the main event. We considered an $M_w = 3.5$, equivalent to an $M_0 = 2.24 \times 10^{14}$ N m, for the main event according to the relationship $M_w - m_R$ established above (Section 3.3). We calculated a stress drop of 0.33 MPa, which is well below the median value from Allmann & Shearer (2009) for intraplate earthquakes (median of 5.53 ± 1.01 MPa) for magnitudes greater than 5, although it is still within the observed range (>0.3 MPa).

An independent spectral analysis (Drouet & Assumpção 2013; Drouet, personal communication, 2013) indicates a corner frequency of $f_c = 1.5 \pm 0.1$ Hz for the main shock. Using the equation proposed by Madariaga (1976), and the k constant value for S wave proposed by Kaneko & Shearer (2014), the main shock rupture would correspond to a circular source radius of 0.6 km, leading to a stress drop of 0.45 MPa, which is comparable with our estimate. According to the values empirically obtained by Abercrombie & Leary (1993), earthquakes of this magnitude and rupture areas have stress drops of 0.1–1 MPa. In addition, lower stress drops are expected at shallow depths where vertical loading is lower. In any case, this is a rough calculation that should be cautiously used: an overestimation of the rupture area determined by the aftershocks distribution (because of location uncertainties and/or aftershocks laying outside the fault plane) easily leads to an underestimation of the stress drop value.

Although the prevalent faults and lineaments mapped in the area trend NE–SW (Fig. 1), the seismogenic structure found in this work corresponds to an NNW–SSE-striking plane, which could be an inherited structure of the São Francisco Craton reactivated under the current E–W compressive stress regime that governs this area of Brazil (Assumpção 1992, 1998b; Coblenz & Richardson 1996). In this regard, the P -axes for the focal mechanisms obtained in this work (nearly horizontal P -axes NE to ENE-oriented; Fig. 7) are consistent with the expected stress direction.

Fig. 7 shows the published focal mechanism for the São Francisco Craton and nearby areas. Some observations are noteworthy from this figure: (1) the common occurrence of reverse faulting earthquakes in the central portion of the São Francisco Craton, (2) the relatively homogeneous orientation of P -axes for reverse-faulting earthquakes in the São Francisco Craton and (3) the apparent rotation of P -axes of the two earthquakes west of the São Francisco Craton (Brasilia and Mara Rosa earthquakes) compared to those in the craton. Two events are not enough to define the complete stress directions, but a hydraulic-fracturing measurement near Mara Rosa, at ~100–200 m depth (Caproni & Armelin 1990; blue bar in Fig. 7), also indicates an NW–SE oriented SHmax.

To characterize the stress field in the São Francisco Craton and revisit previous studies on this matter, we inverted the 2012 Montes Claros main shock focal mechanism and other mechanisms available in the literature to obtain the stress tensor of the area. The stress tensor is defined as the orientation of the three principal axes of the stress ellipsoid (σ_1 , σ_2 , σ_3), and the ratio ϕ or ‘shape factor’ which expresses the relationship of σ_2 with respect to σ_1 and σ_3 and is defined as $\phi = (\sigma_2 - \sigma_3)/(\sigma_1 - \sigma_3)$ (Angelier 1979), where σ_1 , σ_2 and σ_3 are the maximum, intermediate and minimum compressional principal stresses, respectively. For the inversion, we combined our mechanism with those of the Manga 1990

earthquake (Assumpção *et al.* 1990), the Correntina 2003 earthquake (Lopes 2008) and the Caraibas-Itacarambi 2007 earthquake (Chimpliganond *et al.* 2010), all of which occurred in the central portion of the São Francisco Craton (Fig. 7, events 1–4). Except for the Correntina event, the fault plane is known (discriminated from the auxiliary plane), and in all cases, dips to the E. The inversion was performed using the code by Michael (1987), which allows to grid-search the best stress tensor for a group of focal mechanisms, even if the fault planes are not known (i.e. both nodal planes are indistinctly considered in the inversion). Given the low number of focal mechanisms and the shallow depths of all of the events (less than ~4 km) in relation to the size of the area, the principal stress directions were constrained to be horizontal and vertical. Furthermore, the mismatch between the observed and calculated rakes for each fault plane is shown in Fig. 8.

The results of the inverted focal mechanisms (Fig. 8, Test 1) show that the four considered earthquake series could be attributed to the same compressional stress field with a maximum compressional stress axis (σ_1) oriented EW, while the least compressional axis (σ_3) is disposed vertically. The calculated shape factor is $\phi = 0.6$, indicating that σ_2 (oriented ~N–S, horizontally) is compressional and roughly 2/3 the value of σ_1 . Although the orientation of σ_1 is the same as that observed by Assumpção (1998a) for a group of four earthquakes in the southern portion of the São Francisco Craton (Fig. 7), the stress regime is different. The minimum horizontal stress is compressional (SHmin = σ_2) for the central part of the craton (this study), whereas SHmin is extensional (σ_3) for the events in the southern part of the craton (Assumpção 1998a).

The heterogeneous stress field for central Brazil is confirmed by the higher rms rake misfit obtained from stress inversions for other combinations of the events as shown in Fig. 8:

Test 1: Four events (numbers 1–4) in the central part of the craton. rms rake misfit = 16.8°, σ_1 = EW and σ_3 = vertical.

Test 2: Including event no. 5 (Encruzilhada, east of the craton). rms misfit = 15.5°, and σ_1 is oriented EW. This shows that event no. 5 is consistent with the same stress field of the central part of the craton.

Test 3: Four events in the centre of the craton (1–4), one in the east (5) and the two events in the west (6,7). rms rake misfit = 16.0° and σ_1 oriented NW–SE. This shows that the few focal mechanisms currently available for the west part of the craton (events 6 and 7) do not allow the stress field of the central portion of the craton to be distinguished from that of the Brasilia fold belt to the west.

Test 4: Five events in central craton (1–5) with five events in the south (8–12). rms rake misfit = 38.6°. This shows that the stress regime in the southern part of the craton is different from that in the central part.

These results show that the stress field in the craton and surrounding areas is not uniform. Compressional stresses (σ_3 vertical) predominate in the central part of the craton as well as in central Brazil, west of the craton. Strike-slip stresses (σ_1 = EW, σ_3 = NS) predominate in the southern part of the craton and adjacent fold belts. The few available focal mechanisms do not constrain the σ_1 orientation in the central part of the craton: a compressional stress field with an NW–SE oriented σ_1 (in agreement with the hydraulic fracturing measurement in Fig. 7) would explain most focal mechanisms in the central part of the craton just as well. However, the consistent ~E–W orientation of the P -axes in the central part of the craton (Fig. 7) and the large residuals of the two best determined focal mechanisms (Montes Claros 2012 and Caraibas 2007;

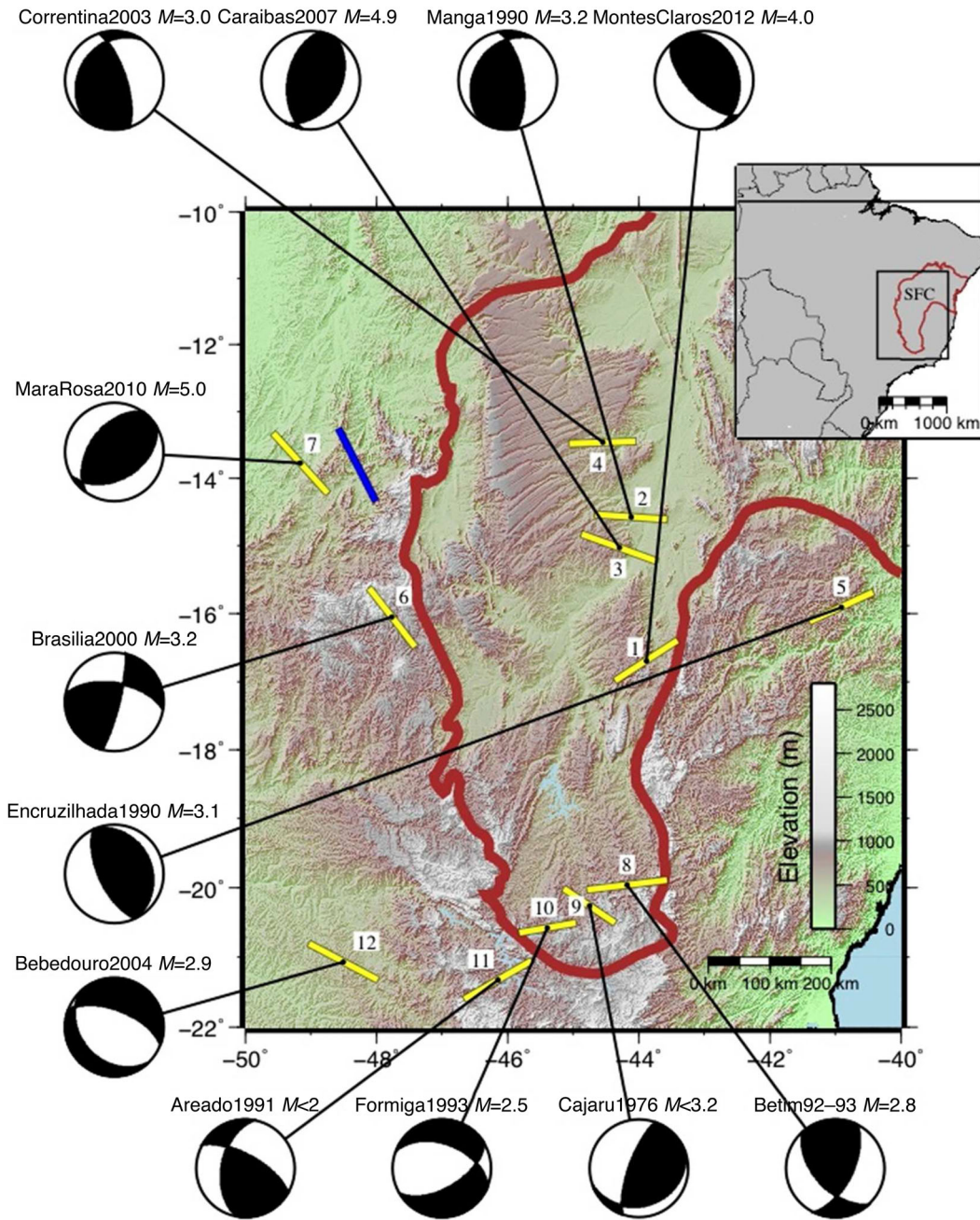


Figure 7. Published focal mechanisms for the São Francisco Craton (thick brown line) and nearby areas. Yellow bars show the orientations of P -axes, except for the Formiga and Bebedouro earthquakes, for which the B -axis is shown. The blue bar shows the SH_{max} *in situ* measurement (Caproni & Armelin 1990). Sources of focal mechanisms anticlockwise from the Montes Claros earthquake: this study; Assumpção *et al.* (1990); Chimpliganond *et al.* (2010); Lopes (2008); Barros *et al.* (2011); Fábio Dias, personal communication, 2013; Veloso (1990); Gabriel Dicelis, personal communication, 2014. The four events in the southern São Francisco Craton (8–11) are all from Assumpção (1998a).

Fig. 8) suggest a possible rotation of σ_1 from $\sim E-W$ in the craton to $NW-SE$ in central Brazil. This issue would require additional studies to be resolved.

Assumpção (1998b) showed that the $E-W$ orientation of σ_1 and the strike-slip stress regime near the southern border of the São Francisco Craton were consistent with the numerical models of intraplate stresses from Coblenz & Richardson (1996) and Meijer (1995). The $E-W$ compressional stress arises mainly from the Mid-Atlantic ridge-push force and the collision between the Nazca

and South America plates, with an $N-S$ extensional component because of continental spreading along the SE continental margin. However, neither regional models (Coblenz & Richardson 1996; Meijer 1995) nor global models of intraplate stresses (e.g. Lithgow-Bertelloni & Guynn 2004) show large stress regime variations over short distances, as observed near the São Francisco Craton.

It is also important to mention that the compressional stress field for the central São Francisco Craton differs from the governing stresses in NE Brazil where density contrasts and sediment loading

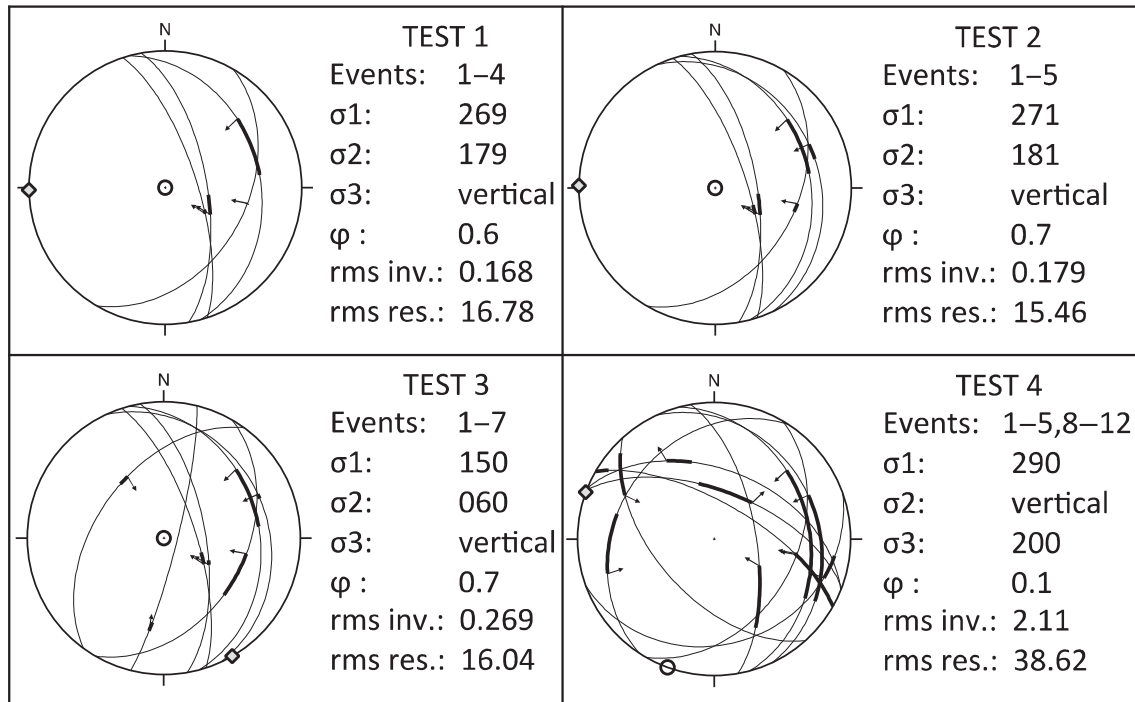


Figure 8. Results from stress inversion tests. Diamonds and circles indicate the azimuth of σ_1 and σ_3 , respectively. The fault planes and their sense of slip (arrows) of the considered focal mechanisms are shown. Differences between the observed and calculated rakes are given by the thick black segments on the planes. See text for details.

along the continental margin produce local N–S oriented extensional stresses favouring strike-slip faulting (e.g. Assumpção 1992, 1998b; Ferreira *et al.* 1998).

In some stable continental regions, such as central and eastern North America and NE Asia, the stress field is uniform over a scale of ~ 2000 km (Coblentz & Richardson 1995; Heidbach *et al.* 2010), suggesting a predominance of plate-boundary forces as sources of intraplate stresses. However, in regions such as western Europe, a short-wavelength pattern (< 200 km) is observed, indicating a greater importance of regional/local sources of stress (Heidbach *et al.* 2010). Similarly, the non-uniformity of stresses in central Brazil highlight the importance of local sources of stress, with a contribution comparable to that of the plate-scale tectonic forces affecting South America. For example, part of the suggested stress field rotation between the central portion of the São Francisco Craton and central Brazil could result from local NW–SE compressional stresses due to flexural crustal loads (Assumpção & Sacek 2013).

Because the few stress data available in Brazil do not allow a definitive characterization of the stress field wavelengths in mid-plate South America, this study suggests a possible rotation of the maximum horizontal stress direction in central-east Brazil, highlighting the importance of local studies to accurately assess the distribution of tectonic stresses.

5 CONCLUSION

The 2012 May 19 Montes Claros earthquake and its aftershock sequence had a tectonic origin associated with the compressional stress field dominant in the central part of the São Francisco Craton. The main shock had a magnitude $m_R = 4$ and the largest aftershocks had magnitudes up to $M_W = 3.1$ ($m_R = 3.6$). The seismicity nucleated at depths of 0.5–1.5 km, defining an NNW-trending plane,

dipping to the E. This agrees with the computed focal mechanism for the main shock and moment tensors calculated for some of the aftershocks. This structure had not been previously recognized in the area and could correspond to an inherited structure within the cratonic basement reactivated under the current compressive stress regime.

Historical records suggest that the area near Montes Claros is regularly shaken by earthquakes of $m \sim 4$. Therefore, the recent sequence may be part of the normal accommodation of stresses in the area with no direct relationship with the quarry blasts near the town. Nevertheless, considering the shallow depths of the natural seismicity, we cannot completely discard the possibility of some inductive mechanism related to the mining activities. One possible link could be that removal of large volumes of rocks from the surface would reduce vertical stresses (σ_3), thus increasing differential stresses in a compressional regime. To test this hypothesis requires additional studies.

The orientation and reverse faulting nature of the seismicity are similar to other focal mechanisms in the central part of the São Francisco Craton, complementing previous studies on the regional stress field. All considered earthquakes in the central part of the craton and in the Brasilia belt are caused by compressional stresses (vertical σ_3). It is not clear if a single NW–SE orientation of the compressional field spans the whole area (less likely), or if σ_1 rotates from E–W in the craton to NW–SE in the west, which is more likely. Moreover, the events located around the southern border of the craton occur under a different stress field, highlighting the contribution of local sources of stresses in mid-plate South America.

ACKNOWLEDGEMENTS

We thank the Municipality of Montes Claros for field support, and especially Mattson Malveira from the local Civil Protection Agency;

Luis Galhardo Filho (USP), Marcelo Moreira (UnB) and Manoel Leite (Univ. de Montes Claros) for field work and general support and Mônica Von Huelsen (UnB) for useful discussions. We also thank Fábio Dias and Gabriel Dicelis for the unpublished focal mechanisms of the Brasília and Bebedouro events, respectively. We thank all land owners for allowing station installation. We also thank the mining companies JLX (Eng. Hamilton, and Vanildo Lima), Lafarge (Joelcio Constatino, and Elbas Pegorari) and Sobritas (Christian Almeida) for information on their explosion activities. We thank Francisco H. Bezerra and an anonymous reviewer for greatly improving our manuscript. This work is part of the Petrobras funded BRASIS project. Some of the figures were made with the software GMT (Wessel & Smith 1998).

REFERENCES

- Abercrombie, R.E. & Leary, P.C., 1993. Source parameters of small earthquakes recorded at 2.5 km depth, Cajon Pass, southern California: implications for earthquake scaling, *Geophys. Res. Lett.*, **20**, 1511–1514.
- Aki, K., 1972. Earthquake mechanism, *Tectonophysics*, **13**(1–4), 423–446.
- Albuquerque, D.F., Assumpção, M., França, G.S., Von Huelsen, M.G., Barbosa, J.R. & Galhardo, L., 2012. Estudos preliminares da sismicidade registrada em Montes Claros, Minas Gerais, Expanded abstract, *V Simpósio Brasileiro de Geofísica*, Salvador, Brazil, 27–29 November 2012.
- Allmann, B.B. & Shearer, P.M., 2009. Global variations of stress drop for moderate to large earthquakes, *J. geophys. Res.*, **114**, doi:10.1029/2009JB005821.
- Almeida, F.F.M. de, Brito Neves, B.B. & Carneiro, C.D.R., 2000. The origin and evolution of the South American Platform, *Earth Sci. Rev.*, **50**(1–2), 77–111.
- Angelier, J., 1979. Determination of the mean principal directions of stresses for a given fault population, *Tectonophysics*, **56**, T17–T26.
- Assumpção, M., 1983. A regional magnitude scale for Brazil, *Bull. seism. Soc. Am.*, **73**(1), 237–246.
- Assumpção, M., 1992. The regional intraplate stress field in South America, *J. geophys. Res.*, **97**, 11 889–11 903.
- Assumpção, M., 1998a. Focal mechanisms of small earthquakes in the southeastern Brazilian shield: a test of stress models of the South American plate, *Geophys. J. Int.*, **133**, 490–498.
- Assumpção, M., 1998b. Seismicity and stresses in the Brazilian passive margin, *Bull. seism. Soc. Am.*, **78**(1), 160–169.
- Assumpção, M. & Sacek, V., 2013. Intra-plate seismicity and flexural stresses in central Brazil, *Geophys. Res. Lett.*, **40**, 487–491.
- Assumpção, M. & Suárez, G., 1988. Source mechanisms of moderate-size earthquakes and stress orientation in mid-plate South America, *Geophys. J.*, **92**, 253–267.
- Assumpção, M., Suárez, G. & Veloso, J.A.V., 1985. Fault plane solutions of intraplate earthquakes in Brazil: some constraints on the regional stress field, *Tectonophysics*, **113**, 283–293.
- Assumpção, M., Veloso, J.A.V., Barbosa, J.R., Blum, M.L.B., Carvalho, J.M., Neves, E. & Bassini, A., 1990. The Manga earthquakes, MG, March of 1990, in *Proceedings of the XXXVI Brazilian Congress of Geology*, Vol. 6, SBG, Natal-RN, pp. 2154–2159.
- Assumpção, M. *et al.*, 2013. The 2012 Montes Claros earthquake sequence in the São Francisco craton: another evidence of inverse faulting and compressional stresses in Eastern Brazil, in *Proceedings of 13th Int. Congr. of the Brazilian Geophys. Soc.*, Rio de Janeiro, Brazil, August 26–29, 2013.
- Assumpção, M. *et al.*, 2014. Intraplate seismicity in Brazil, in *Intraplate Earthquakes*, chap. 3, ed. Talwani, P., Cambridge Univ. Press.
- Barros, L.V., Assumpção, M., Quintero, R. & Caixeta, D., 2009. The intraplate Porto dos Gaúchos seismic zone in the Amazon craton – Brazil, *Tectonophysics*, **469**, 37–47.
- Barros, L.V., Chimpliganond, C.N., Von Huelsen, M.G., Franca, G.S.L.A., Caixeta, D.F. & Albuquerque, D.F., 2011. The Mara Rosa 5.0 mb earthquake and aftershock activity, in *Proceedings of XII International Congress of the Brazilian Geophysical Society, 2011*, Rio de Janeiro. [Anais do XII Congresso Internacional da Sociedade Brasileira de Geofísica.]
- Berrocail, J., Assumpção, M., Antezana, R., Dias Neto, C., Ortega, R., França, H. & Veloso, J.A., 1984. *Sismicidade do Brasil*, IAG/USP and Comissão Nacional de Energia Nuclear, 320 pp.
- Caproni, N. Jr. & Armelin, J.L., 1990. Instrumentação das escavações subterrâneas da UHE Serra da Mesa, in *Simpósio sobre Instrumentação Geotécnica de Campo - SINGEO'90*, Vol. 1, Associação Brasileira de Geologia de Engenharia, São Paulo, pp. 249–257.
- Chaves, M.L.S.C., Andrade, K.W. & Benitez, L., 2011. Geologia integrada das Folhas Jequitai, Bocaiúva e Montes Claros (1:100.000), norte de Minas Gerais, *Geonomos*, **19**(2), 1–7.
- Chimpliganond, C., Assumpção, M., Von Huelsen, M. & França, G.S., 2010. The intracratonic Caraíbas–Itacarambi earthquake of December 9, 2007 (4.9 mb), Minas Gerais State, Brazil, *Tectonophysics*, **480**(1–4), 48–56.
- Ciardelli, C., Assumpção, M. & Agurto-Detzel, H., 2014. Study of the Montes Claros seismogenic fault, in the Sao Francisco craton, Brazil, with correlations of *P*- and *S*-wave phases, *Earth Sci. Res. J.*, **18**(Special Issue [July, 2014]), 100.
- Coblentz, D. & Richardson, R.M., 1995. Statistical trends in the intraplate stress field, *J. geophys. Res.*, **100**(B10), 20 245–20 255.
- Coblentz, D.D. & Richardson, R.M., 1996. Analysis of the South American intraplate stress field, *J. geophys. Res.*, **101**, 8643–8657.
- Cordani, U.G., Sato, K., Teixeira, W., Tassinari, C. & Basel, M.A., 2000. Crustal evolution of the South America platform, in *Tectonic Evolution of South America*, pp. 41–95, eds Cordani, U.G., Thomaz filho, A. & Milani, J., CPRM.
- Drouet, S. & Assumpção, M., 2013. Spectral analysis of Brazilian data and comparison with ground-motion models, in *Proceedings of the 13th International Congress of the Brazilian Geophysical Society, Rio de Janeiro, Brazil*, August 26–29, 2013.
- Eshelby, J., 1957. The determination of the elastic field of an ellipsoidal inclusion, and related problems, *Proc. R. Soc. Lond., A*, **241**(1226), 376–396.
- Ferreira, J.M., Oliveira, R.T., Takeya, M.K. & Assumpção, M., 1998. Superposition of local and regional stresses in northeast Brazil: evidence from focal mechanisms around the Potiguar marginal basin, *Geophys. J. Int.*, **134**, 341–355.
- Havskov, J. & Ottemöller, L., 1999. SeisAn earthquake analysis software, *Seismol. Res. Lett.*, **70**, 532–534.
- Heidbach, O., Tingay, M., Barth, A., Reinecker, J., Kurfeß, D. & Müller, B., 2010. Global crustal stress pattern based on the World Stress Map database release 2008, *Tectonophysics*, **482**, 3–15.
- Heineck, C.A. *et al.*, 2004. Folha SE.23-Belo Horizonte, in *Carta Geológica do Brasil ao Milionésimo, Programa Geologia do Brasil – PGB*, eds Schobbenhaus, C. *et al.* CPRM, Brasília. CD-ROM.
- Johnston, A.C., 1989. Seismicity of stable continental interiors, in *Earthquakes at North-Atlantic Passive Margin: Neotectonics and Postglacial Rebound*, pp. 299–327, eds Gregersen, S. & Basham, P.W., Kluwer.
- Kanamori, H. & Anderson, D., 1975. Theoretical basis of some empirical relations in seismology, *Bull. seism. Soc. Am.*, **65**(5), 1073–1095.
- Kaneko, Y. & Shearer, P.M., 2014. Seismic source spectra and estimated stress drop from cohesive-zone models of circular subshear rupture, *Geophys. J. Int.*, **197**, 1002–1015.
- Kissling, E., Ellsworth, W.L., Eberhart-Phillips, D. & Kradolfer, U., 1994. Initial reference models in local earthquake tomography, *J. geophys. Res.*, **99**, 19 635–19 646.
- Lienert, B.R. & Havskov, J., 1995. A computer program for locating earthquakes both locally and globally, *Seismol. Res. Lett.*, **66**(5), 26–36.
- Lithgow-Bertelloni, C. & Guynn, J.H., 2004. Origin of the lithospheric stress field, *J. geophys. Res.*, **109**, B01408, doi:10.1029/2003JB002467.
- Lopes, A.E.V., 2008. Focal mechanisms and lithospheric stresses in Brazil, *PhD thesis*, IAG, University of São Paulo, 300 pp (in Portuguese).
- Madariaga, R., 1976. Dynamics of an expanding circular fault, *Bull. seism. Soc. Am.*, **66**(3), 639–666.

- Meijer, P.T., 1995. Dynamics of active continental margins: the Andes and the Aegean region, *PhD thesis*, Utrecht University, the Netherlands, 218 pp.
- Michael, A.J., 1987. Use of focal mechanisms to determine stress: a control study, *J. geophys. Res.*, **92**, 357–368.
- Nuttli, O., 1983. Average seismic source-parameter relations for mid-plate earthquakes, *Bull. seism. Soc. Am.*, **73**(2), 519–535.
- Pirchiner, M., Collaço, B., Calhau, J., Assumpção, M. & Dourado, J.C., 2011. The BRAzilian Seismographic Integrated Systems (BRASIS): infrastructure and data management, *Ann. Geophys.*, **54**(1), 17–22.
- Sokos, E. & Zahradnik, J., 2008. ISOLA: a Fortran code and a MATLAB GUI to perform multiple-point source inversion of seismic data, *Comput. Geosci.*, **34**(8), 967–977.
- Talwani, P. & Rajendran, K., 1991. Some seismological and geometric features of intraplate earthquakes, *Tectonophysics*, **186**(1–2), 19–41.
- Veloso, J.A.V., 1990. Atividade sísmica de Encruzilhada-BA, in *Proceedings of 36th Brazilian Congresso of Geology*, Natal (in Portuguese).
- Viegas, G.M., Abercrombie, R.E. & Kim, W.-Y., 2010. The 2002 M5 Au Sable Forks, NY, earthquake sequence: source scaling relationships and energy budget, *J. geophys. Res.*, **115**, B07310, doi:10.1029/2009JB006799.
- Wells, D.L. & Coppersmith, K.J., 1994. New empirical relationships among magnitude, rupture length, rupture width, rupture area, and surface displacement, *Bull. seism. Soc. Am.*, **84**, 974–1002.
- Wessel, P. & Smith, W., 1998. New, improved version of generic mapping tools released, *EOS, Trans. Am. geophys. Un.*, **79**, 579.

SUPPORTING INFORMATION

Additional Supporting Information may be found in the online version of this article:

Table S1. List of events located in the Montes Claros area up to the main shock of 2012.

Figure S1. Largest events occurred in Montes Claros since 1995.

Figure S2. Composite Wadatti diagram computed with a selection of 102 events (482 *P* + 482 *S* arrivals).

Figure S3. (a) Temporal evolution of the seismic sequence. (b) Epicentres coloured by hour of occurrence.

Figure S4. Waveform fitting for moment tensor full waveform inversion of event 2012 September 12 23:56 hr.

Figure S5. Waveform fitting for moment tensor full waveform inversion of event 2012 November 15 03:03 hr.

Figure S6. Waveform fitting for moment tensor full waveform inversion of event 2012 December 19 04:54 hr.

Figure S7. Examples of seismograms for different sources. (<http://gji.oxfordjournals.org/lookup/suppl/doi:10.1093/gji/ggu333/-/DC1>).

Please note: Oxford University Press is not responsible for the content or functionality of any supporting materials supplied by the authors. Any queries (other than missing material) should be directed to the corresponding author for the article.